Cellular Signalling 44 (2018) 148–157

Contents lists available at ScienceDirect

Cellular Signalling

journal homepage: www.elsevier.com/locate/cellsig

# Intracellular zinc increase affects phosphorylation state and subcellular localization of protein kinase C delta (δ)

Kira G. Slepchenko[a,*], Justin M. Holub[b,c,d], Yang V. Li[a,*]

[a] Department of Biomedical Sciences, Heritage College of Osteopathic Medicine, Ohio University, Athens, OH 45701, USA
[b] Department of Chemistry and Biochemistry, Ohio University, Athens, OH 45701, USA
[c] Molecular and Cellular Biology Program, Ohio University, Athens, OH 45701, USA
[d] Edison Biotechnology Institute, Ohio University, Athens, OH 45701, USA

ARTICLE INFO

*Keywords:*
Protein kinase C delta
Intracellular zinc
Phosphorylation
Protein structure

ABSTRACT

Protein kinase C delta (PKCδ) is a Ser/Thr-specific kinase involved in many fundamental cellular processes including growth, differentiation and apoptosis. PKCδ is expressed ubiquitously in all known cell types, and can be activated by diacylglycerol, phorbol esters and other kinases. Multiple lines of evidence have indicated that the mode of activation greatly influences the role PKCδ plays in cellular function. Divalent metal ions, such as zinc are released as a response to cellular stress and injury, often resulting in oxidative damage and cell death. In this study, we evaluate the effect increased concentrations of intracellular zinc has on the phosphorylation state and subcellular localization of PKCδ. More specifically, we demonstrate that intracellular zinc inhibits the phosphorylation of PKCδ at $Thr^{505}$ in a concentration-dependent manner and facilitates the translocation of PKCδ from the cytosol to the Golgi complex. Analysis of a PKCδ structural model revealed a potential His-Cys3 zinc-binding domain adjacent to residue $Thr^{505}$ and suggests that interaction with a $Zn^{2+}$ ion may preclude phosphorylation at this site. This study establishes zinc as a potent modulator of PKCδ function and suggests a novel mechanism by which PKCδ is able to "sense" changes in the concentration of intracellular zinc. These findings illuminate a new paradigm of metal ion-protein interaction that may have significant implications on a broad spectrum of cellular processes.

## 1. Introduction

Protein kinase C delta (PKCδ) is a member of the PKC family of Ser/Thr kinases that are expressed in brain, heart, spleen, lung, liver, ovary, pancreas and adrenal gland [1, 2]. PKCδ activity has been implicated in a wide range of cellular processes including proliferation [3, 4], differentiation [5] and apoptosis [6–8]. Structurally, PKCδ consists of a C-terminal catalytic domain and N-terminal regulatory domain [9, 10]. Together with PKC ε, η and θ, PKCδ is classified as a 'novel kinase', which can be activated by diacylglycerol (DAG) or phorbol esters and is calcium-independent [11]. PKCδ is the most well-studied novel protein kinase, and it has recently been discovered that PKCδ can have both pro- and anti-apoptotic function [6, 12]. Despite these advancements however, a consensus on the functional nature of PKCδ remains to be established. This disparity likely exists because the activity of PKCδ is highly dependent on cell type, phosphorylation state, external stimuli and intracellular localization [10, 13, 14].

The biological functions of proteins within the PKC family are primarily controlled by their subcellular localization [13, 15, 16] and phosphorylation state [17]. Aside from being activated by DAG and phorbol esters, PKCδ can also be activated by other kinases. Regulation of PKCδ function by phosphorylation is quite complex [17]; PKCδ has been shown to be phosphorylated at up to 17 sites, including eight Ser/Thr residues and nine Tyr residues [18]. Several of these sites, such as $Ser^{643}$ and $Ser^{662}$, remain constitutively phosphorylated and have little known effect of PKCδ function [18]. Conversely, phosphorylation of PKCδ within its C-terminal domain activation loop at $Thr^{505}$ has been associated with increased kinase activity [18]. PKCδ is unique from all the other kinases in the novel kinase subfamily, because it does not require phosphorylation at $Thr^{505}$ for catalytic function [19]. These observations have led to speculation that phosphorylation at $Thr^{505}$ ($pThr^{505}$) is used to fine-tune PKCδ substrate specificity [19, 20]. The complex nature of PKCδ phosphorylation may explain the multifaceted and stimulus-depended functions of PKCδ, making it an interesting target for investigation.

Zinc is the most abundant intracellular trace mineral, being found in the cytosol, organelles and nucleus of all cell types [21]. Zinc is required for the function of hundreds of enzymes [22] and is crucial for

* Corresponding authors.
*E-mail addresses:* slepchen@ohio.edu (K.G. Slepchenko), liy1@ohio.edu (Y.V. Li).

https://doi.org/10.1016/j.cellsig.2018.01.018
Received 27 November 2017; Accepted 14 January 2018

stabilizing the folded structure of many non-enzymatic proteins [23]. Zinc is unique among transition metals in that it is redox inert in biological systems and has only one valence state: Zn(II) [24]. The electron donors such as oxygen, nitrogen and sulfur limit zinc interactions with proteins [24]. As a cofactor, zinc may remain bound during the lifetime of proteins that rely on it for catalytic function. Other proteins, however, may bind free zinc reversibly with dissociation rates corresponding with functional requirements. These dissimilar binding attributes allow zinc to play highly important roles in cell physiology [25, 26]. Despite its inert redox potential, concentrations of intracellular free zinc are tightly regulated through organelle compartmentalization [27] and binding to metallothioneines [25, 28]. This high level of control is achieved by transmembrane proteins that transport zinc in and out of intracellular compartments. Proteins such as Zrt and Irt-like protein function to transport zinc ions ($Zn^{2+}$) into the cytosol from outside the cell or from vesicles, whereas proteins such as ZnT control the efflux of $Zn^{2+}$ from the cytoplasm to outside the cell or into vesicles [29]. While zinc is considered an essential element required for normal physiological function, dysregulated zinc homeostasis has been implicated in pathogenesis of human disease. For example, zinc deficiencies can result in oxidative damage to DNA and lead to increased cancer risk [30]. Furthermore, inefficient zinc transport has been linked to the onset of neurodegenerative diseases [31, 32], depression [33, 34] and type II diabetes [35, 36]. Finally, numerous reports have shown that concentrations of intracellular zinc increase during hypoxia [37–40] and that such increases in zinc can precede cell death in neurons [39]. More recently, zinc has emerged as a potent modulator of protein phosphorylation in cells. Indeed, it has been shown that increases in intracellular zinc concentrations can facilitate the phosphorylation of proteins such as tau [41], insulin-like growth factor receptor [42], and insulin-like growth factor-1 [43]. The inhibitory effects of zinc on protein phosphorylation have also been reported [44] however, less is known about how zinc influences this process.

The current study was designed to investigate how increases in intracellular zinc concentrations affect the phosphorylation state and subcellular trafficking of PKCδ. We report here that increasing concentrations of intracellular free zinc significantly inhibits phosphorylation of PKCδ at a key phosphorylation site: $Thr^{505}$, in a concentration-dependent manner; and influences PKCδ translocation from cytosol to the Golgi complex. We also employed molecular modeling software to gain additional insight into how zinc might affect the structure of PKCδ. These studies show that zinc may bind to a novel His-Cys3 binding pocket that is adjacent to $Thr^{505}$. We therefore propose a mechanism by which PKCδ is able to 'sense' concentrations of intracellular zinc by coordinating it to a His-Cys3 binding site. Importantly, this binding event repositions $His^{197}$ so that it blocks access to $Thr^{505}$, effectively inhibiting phosphorylation at this site. This new paradigm enhances our understanding of zinc·PKCδ interactions and implicates zinc as a potent modulator of PKCδ activity.

## 2. Materials and methods

### 2.1. Reagents and chemicals

Unless otherwise stated, all chemicals were purchased from Sigma-Aldrich (St. Louis, MO). Fluorescent zinc dye, FluoZin-3, AM was purchased from Life Technologies (Waltham, MA). Microscopy supplies were purchased from VWR (Radnor, PA). HeLa cells and cell culture reagents were purchased from ATCC (Manassas, VA). Immunoblot materials were purchased from Bio-Rad (Hercules, CA) and Invitrogen (Waltham, MA). Antibodies were from Cell Signaling Technology (Danvers, MA) and Abcam (Cambridge, MA).

### 2.2. Cell culture

HeLa cells (laboratory passage 4–14) were maintained in Eagle's minimum essential medium (EMEM) supplemented with 5% fetal bovine serum (FBS) under a humidified atmosphere (95%) containing 5% $CO_2$ at 37 °C. Cells were subcultured every other day using standard trypsinization methods, according to ATCC recommendations.

### 2.3. Detection of intracellular free zinc levels

HeLa cells were seeded at medium density onto glass-bottom Petri dishes (P35G-4.5-14-C; MatTek Corp, Ashland, MA). Following seeding, the cells were allowed to incubate under a humidified atmosphere (95%) containing 5% $CO_2$ at 37 °C for at least 24 h before experimentation. Prior to treatments, the cells were washed three times with warm physiological buffer (25 mM HEPES, 125 mM NaCl, 3 mM KCl, 1.28 mM $CaCl_2$, 1.1 mM $MgCl_2$ and 5 mM glucose, pH 7.4). For zinc detection, FluoZin-3, AM was added to the cell media at final concentration of 1 μM and cells were incubated for 60 min at room temperature. After incubation with the dye, cells were washed three times with physiological buffer and allowed to "rest" at room temperature for 30 min. To ensure removal of incident extracellular dye, the cells were washed one final time with physiological buffer before observation by fluorescence microscopy. For treatments, either pyrithione alone or a combination of pyrithione and zinc chloride was added to the media and the cells were allowed to incubate for 10 min at 37 °C. Final concentrations of pyrithione and zinc chloride were 10 μM and 50 μM respectively. Images were collected using a Motic AE31 microscope outfitted with a QImaging Retiga 1300i camera with a 40 × /0.75 Olympus objective. Image-Pro Plus 6.2 (Media Cybernetics) was used to collect and analyze the data. Images were collected every 30 s and zinc was added after 60 s of baseline fluorescence was recorded. To detect changes in intracellular fluorescence, regions of interest (ROI) were selected manually by highlighting areas of the cytosol, excluding the nucleus. Background fluorescence was measured from multiple regions of the same images that contained no cells. Changes in fluorescence (ΔF) were determined using Eq. (1):

$$\Delta F = (F_{measure} - F_0)/F_0 \quad (1)$$

where $F_{measure}$ is measured fluorescence and $F_0$ is average fluorescence at baseline before the application of zinc. Each fluorescent measurement was background subtracted.

### 2.4. PKCδ subcellular localization (western blot)

HeLa cells were seeded at medium density onto 35 mm plastic Petri dishes in 2 mL EMEM supplemented with 5% FBS. Cells were allowed to attach to the plates under a humidified atmosphere (95%) containing 5% $CO_2$ at 37 °C for 24 h before treatments. Immediately prior to treatment, the cells were washed three times with 1 mL of physiological buffer. Depending on experimental conditions, washed cells were then switched to physiological buffer supplemented with either 10 μM pyrithione or 10 μM pyrithione and 50 μM zinc chloride and allowed to incubate for 30 min at 37 °C. All pyrithione and zinc chloride solutions were made fresh before the experiments. Following incubation, the cells were washed with cold PBS and harvested by scraping. The cells were then counted and viable cells were identified using Trypan Blue. Cell number and volumes were adjusted to ensure that control and zinc-treated samples had similar numbers of viable cells. Cells were lysed in cold PBS supplemented with protease inhibitor cocktail (Sigma-Aldrich, P2714) by rapidly passing the cells 20 times through a 27-gauge needle. Lysis efficiency was monitored by observing samples under brightfield microscopy; lysis was deemed complete when no whole cells were observed. Cell homogenates were then centrifuged at 1500 rpm (900 × *g*) at 4 °C for 10 min to pellet unbroken cells and nuclei. The resulting supernatant was then spun at 55,000 rpm (100,000 × *g*) for at 4 °C for 60 min using an Optima TLX Ultracentrifuge (Beckman Coulter, Brea, CA). The supernatant, which contained soluble cytosolic proteins, was heated to 95 °C for 5 min in 1 × Laemmli buffer to prepare the samples

for SDS-PAGE. The resultant pellet, which contained organelles such as fragments of the endoplasmic reticulum, Golgi complex, mitochondria and plasma membrane, was washed with PBS supplemented with protease inhibitors and centrifuged again at 55,000 rpm (100,000 × *g*) for 60 min at 4 °C. Samples were then prepared for SDS-PAGE by heating the resuspended pellet to 95 °C for 5 min in 1 × Laemmli buffer. Subsequent washing and centrifugation of the pellet was performed to reduce contamination by cytosolic proteins. The samples containing whole cell, cytosol and organelle extracts were then loaded onto a 10% polyacrylamide gel and separated by SDS-PAGE using an XCell module (Bio-Rad). Separated proteins were transferred to a 0.45 μm PVDF membrane (Invitrogen) at 300 mA constant voltage for 2 h at room temperature. The membrane was then blocked with 5% bovine serum albumin in tris-buffered saline (TBS) supplemented with 0.1% Tween-20 (TBST) for 2 h at room temperature. Anti-PKCδ [EPR17075] rabbit monoclonal antibody (Abcam, #182126, 1:1000 dilution in 5% BSA/TBST) was used to label PKCδ by incubating the membrane in primary antibody solution overnight with gentle agitation at 4 °C. The membrane was then washed with TBST to remove unbound primary antibody and incubated in a solution containing horse radish peroxidase (HRP)-linked secondary anti-rabbit antibody (Cell signaling Technology, #7074, 1:3000 dilution in 2% BSA/TBST) for 90 min at room temperature with moderate agitation. Membranes were developed using Clarity Western ECL Substrate (Bio-Rad) and signals were detected on a molecular imaging system, ChemiDoc XRS + (Bio-Rad) using ImageLab 3.01 software (Bio-Rad). Total protein staining on the blotted membranes was achieved by incubating membranes in Coomassie brilliant blue R-250 staining solution (Bio-Rad) for 1 min at room temperature. Following staining the membrane was immediately washed 3 times with deionized water and subsequently washed 3 times with deionized water for 10 min each. The washed membrane was dried overnight at room temperature in the dark and imaged using a ChemiDoc XRS + imaging system (Bio-Rad) set to automatic exposure on the colorimetric blot setting using ImageLab 3.01 software (Bio-Rad).

### 2.5. PKCδ subcellular localization (immunofluorescence)

HeLa cells were trypsinized and seeded at medium density onto sterilized glass coverslips (15 mm, #1, Corning) in 35 mm plastic Petri dishes; three coverslips were used per each dish. Cells were plated in 2 mL EMEM supplemented with 5% FBS and were allowed to attach for 24 h under a humidified atmosphere (95%) containing 5% $CO_2$ at 37 °C. Prior to treatments, the cells were washed 3 times with 1 mL of physiological buffer. Following washing, the cells were subjected to pyrithione and zinc treatments as described above. Once the treatments were complete, the coverslips were removed from the Petri dish and the adhered cells were gently washed with physiological buffer. Following washing the cells were immediately fixed by submerging the cover slips in cold (−20 °C) methanol for 5 min. After fixation, the adhered cells were washed with room temperature PBS and permeabilized by submerging the cover slips in room temperature PBS supplemented with 0.1% Triton X-100 for 5 min. After permeabilization the coverslips were submerged in blocking solution (1% BSA, 10% normal goat serum, 0.3 M glycine and 0.1% Tween-20 in PBS) for 1 h at room temperature. Once blocked, the cells were treated with antibodies against PKCδ: anti-PKC delta [EPR17075] rabbit monoclonal antibody (Abcam, #182126, lot GR189581-2, 1:100 dilution in blocking solution), or β-COP: anti-β-COP mouse monoclonal clone maD (Sigma, #G6160, 1:400 dilution in blocking solution). The fixed cells were incubated with primary antibodies overnight at 4 °C without agitation. Following incubation, the adhered cells were washed 4 times with PBS supplemented with 0.1% Tween-20 and incubated with appropriate secondary antibodies (1:400 dilution in blocking solution) for 1 h at room temperature in the dark without agitation. Goat anti-rabbit Alexa 488 (Invitrogen) was used for detection of PKCδ and goat anti-mouse Alexa 546 (Invitrogen) was used for detection of β-COP. Excess secondary antibodies were removed by washing the cover slips 4 times with PBS supplemented with 0.1% Tween-20 at room temperature. The cells were then incubated in PBS containing 1 μg/mL of DAPI (nuclear stain) for 5 min at room temperature. Cells were then washed 3 times with PBS supplemented with 0.1% Tween-20. Each coverslip was then mounted on a glass microscope slide (VWR) using 70% glycerol in PBS. Images were collected immediately on Nikon Fluorescent Microphot–SA microscope outfitted with a 100×/1.3 Nikon objective with ImageQ camera with Qcapture software.

### 2.6. PKCδ phosphorylation (western blot)

HeLa cells were plated and maintained as described above. Briefly, cells were plated on 35 mm culture dishes in 2 mL EMEM supplemented with 5% FBS and were allowed to attach for 24 h. Prior to treatments, cells were washed 3 times with physiological buffer and switched to media supplemented with 10 μM pyrithione and 0, 1, 10 or 50 μM zinc chloride. Cells were then allowed to incubate for 30 min at 37 °C. Following incubation, the treatment solutions were removed and the cells were washed once with physiological buffer. Then, 100 μL of 1.5 × Laemmli sample buffer (Bio-Rad) was added to each culture dish and the cells were scrapped to lift them off the plate. Suspended cells were then transferred to 1.5 mL centrifuge tubes and homogenized on ice using an Eppendorf homogenizer (15 rotations, 1 s each). Following homogenization, the samples were immediately heated to 95 °C for 5 min. The lysate was then loaded onto a 10% polyacrylamide gel and proteins were separated by SDS-PAGE electrophoresis using an XCell II module (Bio-Rad). Proteins were then transferred to a 0.45 μm PVDF membrane using techniques as described above. Following transfer, the membrane was blocked with 5% BSA/TBST for 2 h at room temperature. The membranes were then incubated in BSA/TBST containing antibodies against phospho PKCδ ($pThr^{505}$): anti-phospho PKCδ ($pThr^{505}$) rabbit polyclonal antibody (Cell Signaling Technology, #9374, lot 6, 1:1000 dilution in 5% BSA/TBST) or total PKCδ: anti-PKCδ rabbit polyclonal antibody (Cell Signaling Technology, #2058, lot 1, 1:1000 dilution in 5% BSA/TBST). The membranes were incubated with the primary antibody solution overnight at 4 °C with gentle agitation. Following incubation, the membranes were washed 3 times with TBST to remove unbound primary antibody. The membranes were then incubated with horse radish peroxidase (HRP)-linked secondary anti-rabbit antibody (Cell Signaling Technology, #7074, 1:3000 dilution in 2%BSA/TBST) for 90 min at room temperature with moderate agitation. The excess secondary antibody was removed by washing the membrane 3 times with TBST with moderate agitation. Membranes were developed and bands were detected as described above. Quantification of the band intensity was performed using ImageLab software (Bio-Rad). Each band was highlighted manually and density values were assigned by the program for each protein band. Density values were also quantified from equivalent areas of the blot containing no protein (background) and this value was subtracted from each density value obtained for protein bands. The ratio of total PKCδ to phospho PKCδ ($Thr^{505}$) was calculated and plotted as a percent change of the control.

### 2.7. Molecular modeling

Zinc-binding sites were predicted by uploading the non-redundant human PKCδ sequence (UniProtKB - Q05655) to the ZincExplorer analysis server. Residues with high confidence of zinc-binding included prediction scores between 0.49 and 1 with the higher scores being of greater confidence. To predict the secondary and tertiary structure of the full-length protein, the non-redundant full-length human PKCδ primary sequence (residues 1–676, UniProtKB - Q05655) was uploaded to the PHYRE2 (protein homology/analogy recognition engine V 2.0) server. $Zn^{2+}$ atoms were added to the PKCδ apo-structure using PyMOL

molecular modeling software (Version 1.8 Schrödinger, LLC). The resulting PBD files were then uploaded into the Swiss PDB Viewer (DeepView/Swiss-PDBViewer, Swiss Institute of Bioinformatics) and energy minimizations were performed using a version of the GROMOS 43B1 force field. Minimized protein structures were then visualized and rendered using PyMOL molecular modeling software.

## 3. Results

### 3.1. Concentrations of intracellular zinc increase with addition of exogenous zinc

The capacity to study how zinc affects the biology of PKCδ relied on our ability to systematically raise levels of intracellular zinc in cultured cells. To accomplish this, we labeled HeLa cells with a fluorescent indicator of free zinc: FluoZin-3, AM. This small molecule fluorophore has high affinity for zinc with a dissociation constant ($K_d$) of approximately 15 nM [45]. FluoZin-3, AM exhibits a 50-fold increase in fluorescence in response to saturating levels of zinc. This indicator can be used to monitor changes in cytosolic free/labile zinc, where an increase in intracellular fluorescence represents an increase in concentration of free zinc in the cytosol. As expected, untreated HeLa cells labeled with 1 μM FluoZin-3, AM showed very low basal levels of intracellular free zinc (Fig. 1A). However, when cells were exposed to a combination of 10 μM sodium pyrithione (zinc ionophore) and 50 μM zinc chloride, a significant increase in intracellular fluorescence was observed. Increase in intracellular zinc concentrations appeared to be modest for the first 120 s, followed by a sharp fluorescence enhancement that continued for six minutes. Intracellular zinc levels then stabilized, reaching a plateau that remained relatively constant during the remainder of the 30-min observation (Fig. 1B). Control cells exposed to pyrithione alone did not show an increase in fluorescence, indicating the zinc ionophore alone did not significantly alter the concentration of intracellular free zinc. These results suggest that co-treating cells with exogenous zinc and a zinc ionophore is a reliable method to rapidly and consistently increase intracellular levels of free zinc. Furthermore, this technique may be used to simulate cellular responses to pathological conditions that result in cytosolic zinc increase.

### 3.2. Changes in intracellular zinc affect the subcellular localization of PKCδ

It has been documented that the function of PKCδ is determined by its subcellular localization [13, 15, 46–48]. To investigate whether changes in intracellular free zinc affect the subcellular localization of PKCδ, we treated HeLa cells with 10 μM sodium pyrithione or a combination of 10 μM sodium pyrithione and 50 μM zinc chloride for 30 min and evaluated the subcellular localization of PKCδ by western blot (Fig. 2A). Cells were plated, maintained and treated as described in the Materials and methods. Following treatments, the cells were lysed and subjected to consecutive centrifugation to separate cellular components. For the purpose of this study, the whole cell lysate, before centrifugation was identified as “whole cell”; the supernatant that contained cytosolic proteins was labeled “cytosol”; and the pellet that contained fragments of organelles including the endoplasmic reticulum, Golgi complex, mitochondria and plasma membrane was designated “organelles”. Antibodies specific to PKCδ (Abcam, #182126), were used to visualize the amount of total PKCδ protein in each cellular fraction. As expected, the whole cell lysate showed no significant difference in amount of PKCδ in cells treated with or without zinc (Fig. 2A, upper image). On the other hand, different subcellular localization profiles of PKCδ emerged when the cytosolic and organelle fractions were compared. For example, PKCδ was found to localize to the cytosol in cells that were not exposed to zinc. However, the cytosolic concentration of PKCδ in cells treated with zinc was significantly reduced. It was also observed that PKCδ localizes to cellular organelles even in the absence of zinc, as was indicated by the presence of PKCδ in the organelle fraction of untreated cells. Interestingly, treatment with zinc resulted in a significant increase of PKCδ in the organelle fraction. It

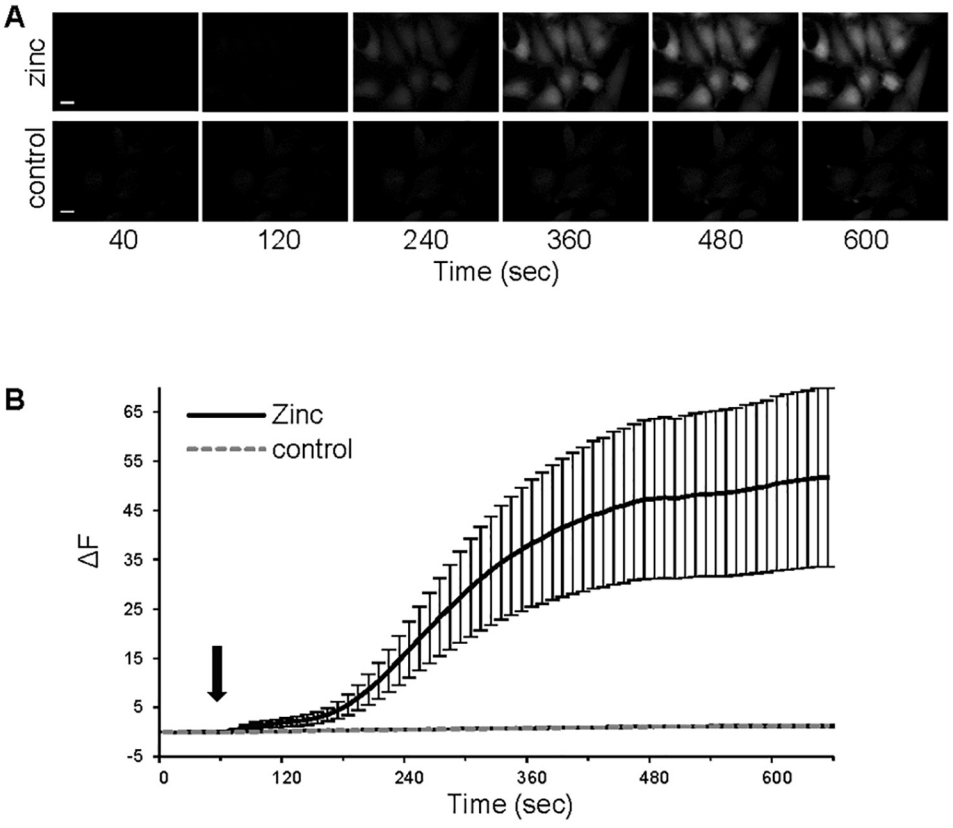


**Fig. 1.** Treatment with exogenous zinc increases concentration of intracellular free zinc in HeLa cells (A) Time-dependent fluorescent micrographs of intracellular zinc increase in live HeLa cells following treatment with 10 μM pyrithione alone (control) or a combination of 10 μM pyrithione and 50 μM zinc chloride (zinc) as detected by FluoZin-3, AM. Numbers under images represent time (seconds) the images were captured post-treatment. Scale bars are 10 μm. (B) Average change in intracellular fluorescence (ΔF) of live HeLa cells treated with 10 μM pyrithione alone (control) or 10 μM pyrithione and 50 μM zinc chloride (zinc) as detected by FluoZin-3, AM. Arrow represents the time of treatment addition at 60 s. Error bars are standard deviation; a total of 15 cells were observed for control treatments, two separate experiments; a total of 9 cells were observed for zinc treatments, two separate experiments.

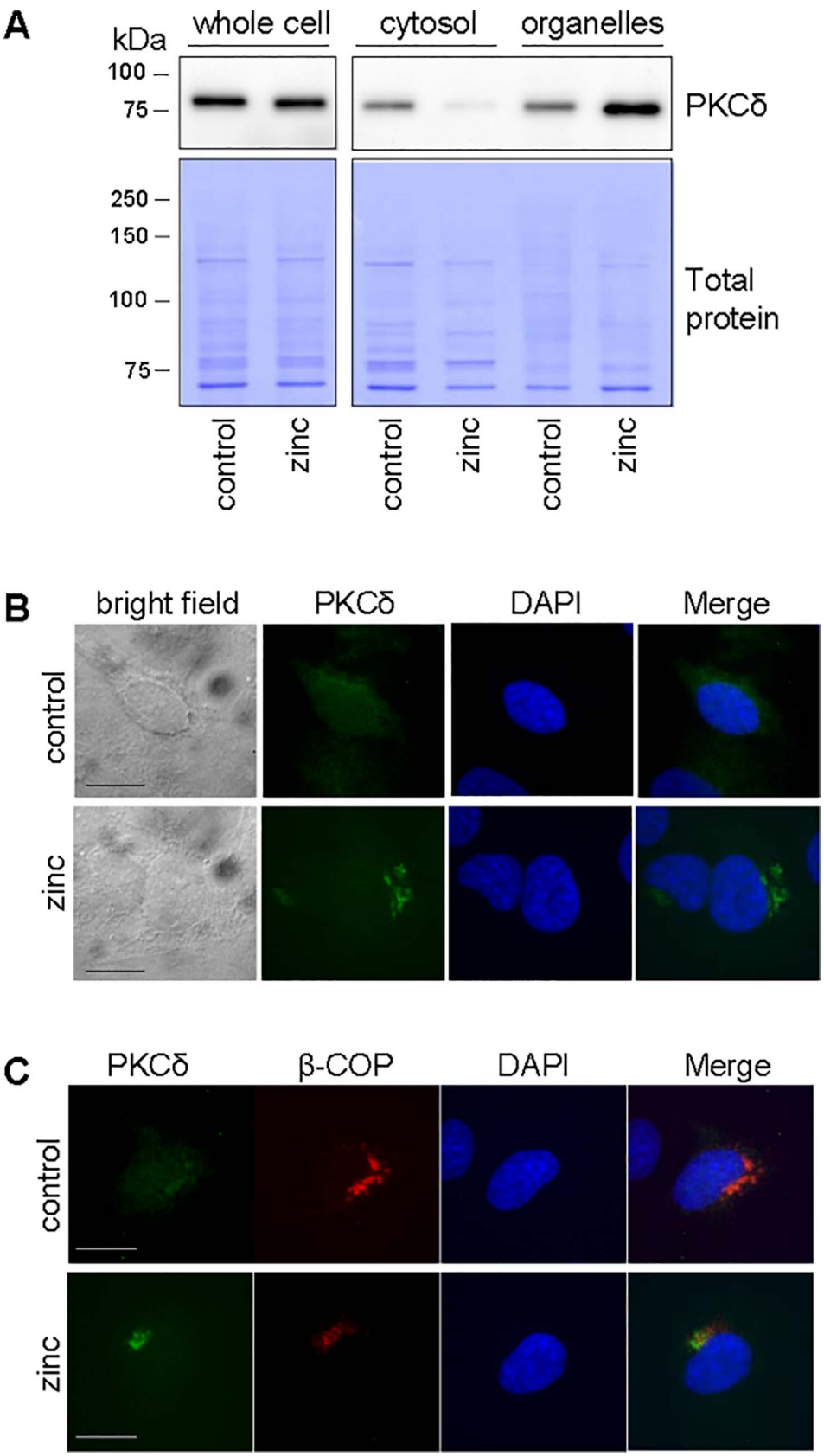


**Fig. 2.** PKCδ translocates from cytosol to Golgi complex upon exposure to zinc (A) Western blot analysis of HeLa cell lysates. Whole cell: whole cell lysate; cytosol: supernatant recovered from high-speed centrifugation of whole cell lysate; organelles: pellet recovered from high-speed centrifugation of whole cell lysate. Size markers (kDa) are shown to the left of the blot images. (B) Immunofluorescence micrographs of HeLa cells. Green fluorescence indicates localization of primary recognizing PKCδ; blue indicates presence of cell nuclei (DAPI stain). Scale bar is 10 μm. (C) Immunofluorescence micrographs of HeLa cells. Green fluorescence indicates localization of primary antibodies recognizing PKCδ; red fluorescence indicates localization of primary antibodies recognizing β-COP; blue indicates presence of cell nuclei (DAPI). Scale bar is 10 μm.

should be noted that the total protein concentration was equivalent between the control and zinc treated cells, as shown by the total protein stain (Coomassie) of the same blot (Fig. 2A, lower image). Taken together, these results suggest that increases in the concentration of intracellular zinc influence the trafficking of PKCδ from the cytosol to organelles or the plasma membrane.

The results from our cellular fractionation experiments strongly suggested that increases in intracellular zinc affect translocation of

PKCδ, however it was not clear from these studies which subcellular compartment PKCδ translocates to. To gain further insight into the zinc-mediated translocation of PKCδ, we treated HeLa cells with 10 μM sodium pyrithione or a combination of 10 μM sodium pyrithione and 50 μM zinc chloride for 30 min and evaluated the subcellular localization of PKCδ by immunofluorescence (Fig. 2B). For these experiments, cells were grown and treated on sterile coverslips used for subsequent immunofluorescent staining (see Materials and methods). Following treatment, the cells were fixed, permeabilized and incubated with primary antibodies against PKCδ (Abcam, #182126). Following treatments with primary antibodies, the cells were washed and incubated with fluorescently-labeled secondary antibodies against the antibodies targeting PKCδ. It was observed from these series of experiments that cells treated with no zinc contained faint and amorphous distribution of PKCδ in the cytosol. Cells treated with zinc contained no observable PKCδ in cytosol and the protein appeared as a bright collection of puncta in the perinuclear region (Fig. 2B). To address whether PKCδ was being targeted to the Golgi complex, HeLa cells were plated on glass coverslips and treated as described above (see Materials and methods). The cells were then fixed, permeabilized and incubated with primary antibodies targeting the Golgi-specific protein β-COP [49] and PKCδ. Following incubation, the cells were washed, and counterstained with fluorescently-labeled antibodies specific for antibodies that targeted β-COP (red) and PKCδ (green) (Fig. 2C). It was seen from these experiments that PKCδ localizes to the Golgi complex in HeLa cells that have been treated with zinc. Collectively, the compartmentalization immunoblot and immunofluorescent data suggest that short (less than 30 min) treatments of exogenous zinc cause PKCδ to traffic from cytosol to the Golgi complex.

### 3.3. Intracellular zinc increase inhibits phosphorylation of PKCδ at Thr$^{505}$

It should be noted that the subcellular location is not the only factor in determining the functional activity of PKCδ. Indeed, phosphorylation is another well-documented modification that controls the activation of this kinase [10]. Several phosphorylation sites on PKCδ are known to affect kinase activity, including Thr$^{505}$, a residue located within the C-terminal activation loop of PKCδ. While phosphorylation at this site has been associated with increased kinase activity, it is not required for catalytic function [18]. To assess how zinc affects the phosphorylation of PKCδ at Thr$^{505}$, we treated cultured HeLa cells with varying concentrations of zinc and assessed pThr$^{505}$ levels by western blot (Fig. 3). HeLa cells were cultured and maintained as described in the Materials and methods. Cells were treated with 10 μM sodium pyrithione and either 0, 1, 10 or 50 μM zinc chloride for 30 min. Following treatments, the cells were lysed and intracellular proteins were separated by SDS-PAGE. Proteins were then transferred to a PVDF membrane and subjected to western blot using antibodies against phosphorylated PKCδ (pThr$^{505}$) or total PKCδ (Fig. 3A). Western blots from these experiments revealed that cells treated with zinc contained significantly less phosphorylated PKCδ. Notably, inhibition of phosphorylation at Thr$^{505}$ was concentration dependent, with 50 μM zinc treatments resulting in the highest level of inhibition. Percent inhibition was quantified by calculating the ratio of normalized phosphorylated PKCδ band intensity between treated and untreated (control) samples (Fig. 3B). Cells treated with 50 μM zinc showed 50.8 ± 4.3% inhibition of phosphorylation at Thr$^{505}$ compared to control cells, whereas 10 and 1 μM zinc treatments showed 43.2 ± 1.6% and 5.8 ± 6.7% inhibition respectively. These data suggest that intracellular zinc increase strongly inhibits phosphorylation of PKCδ at Thr$^{505}$ and that this effect is concentration dependent, with higher zinc concentration showing more pronounced inhibition.

### 3.4. Modeling of PKCδ three dimensional structure complexed with zinc

To gain further insight into which amino acids within the PKCδ sequence can potentially bind zinc, we employed the ZincExplorer web engine [50]. This modeling software can be used to predict potential zinc-binding sites within proteins from their primary sequence. The ZincExplorer web engine consists of a SVM-based predictor, a cluster-based predictor and a template-based predictor. This software assigns zinc-binding prediction scores (0–1) to amino acids based on charge, environment and proximity to other zinc-binding residues. Higher prediction scores are interpreted as having higher probability of binding zinc, where confidence scores of 0.49–1 are considered 66.3% sensitive and 99% specific. To initiate these studies, the primary sequence of full-length PKCδ (residues 1–676, UniProtKB - Q05655) was uploaded to the ZincExplorer web server. The resultant prediction scores were then plotted as a function of amino acid residue (Fig. 4A). Overall, the program selected 16 amino acids in the PKCδ sequence that

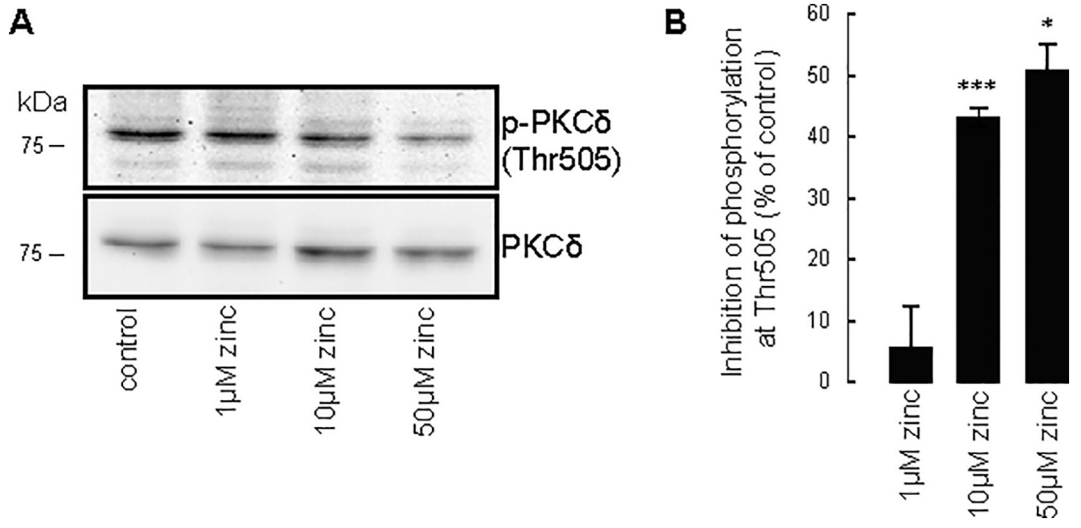


**Fig. 3.** Intracellular zinc inhibits phosphorylation of PKCδ at Thr$^{505}$ (A) Western blot analysis of whole cell lysate from HeLa cells. Size markers (kDa) are shown to the left of the blot images. (B) Column graph showing percent inhibition of phosphorylation as quantified from western blot images. Percent inhibition was quantified by calculating the band intensity ratio of phosphorylated PKCδ in cell lysates treated with zinc to that of untreated (control) samples. Each phosphorylated PKCδ band intensity was normalized to corresponding total PKCδ in the same lane. Error bars are standard deviation (control n = 4; 1 μM zinc n = 2; 10 μM zinc n = 3 and 50 μM zinc n = 4, each n represents a separate experiment and western blot). *P*-values were calculated using comparison of two groups using Student's t-test (single-factor ANOVA); ***, $P = 0.001$ (comparing 1 μM zinc and 10 μM zinc); *, $P = 0.017$ (comparing 10 μM zinc and 50 μM zinc).

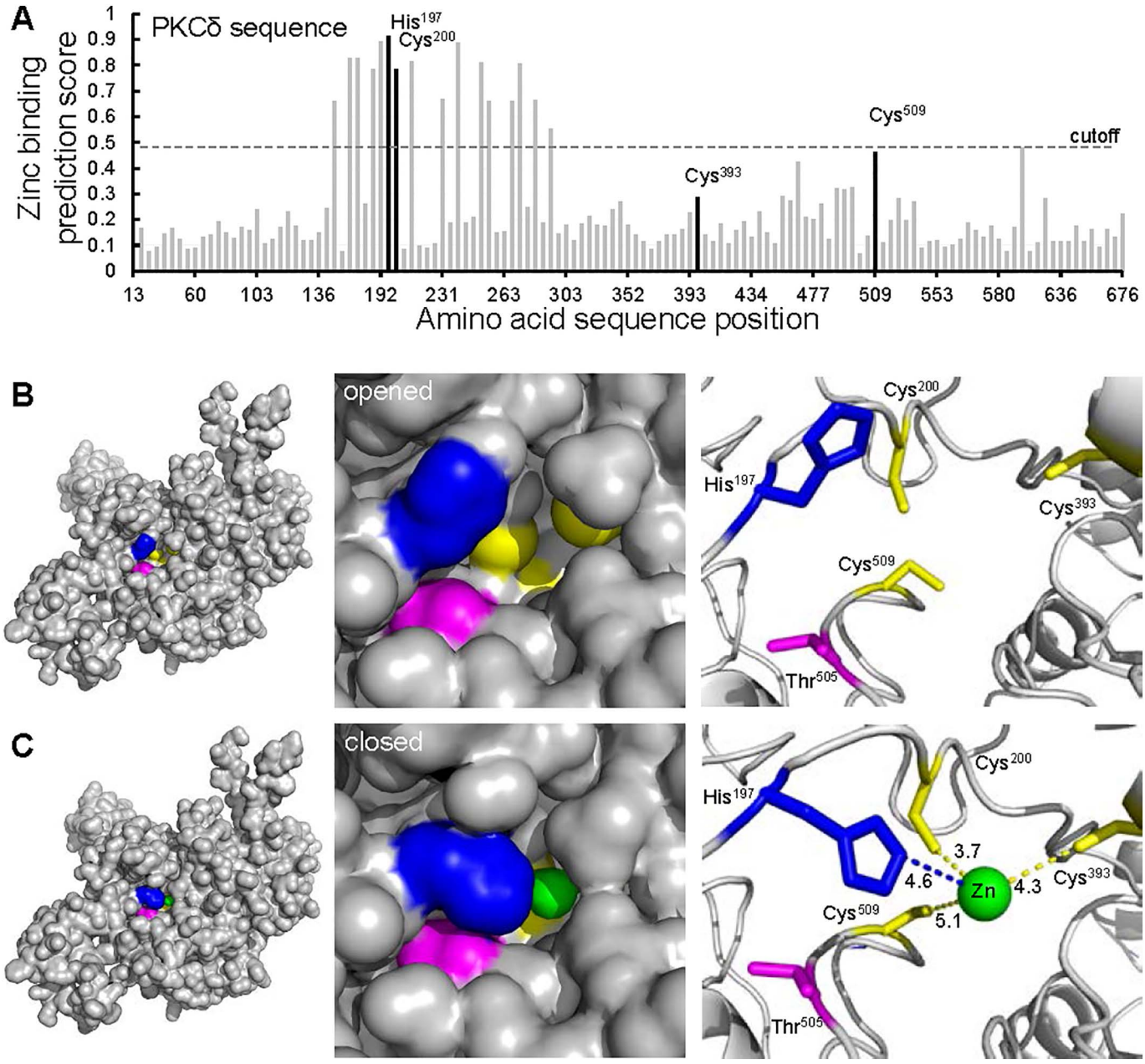


**Fig. 4.** Modeling of zinc ion binding to PKCδ (A) Column graph illustrating zinc binding prediction score for select amino acids within the full-length PKCδ sequence as predicted using Zinc Explorer software. Cutoff value is 0.49. (B) Molecular model of full-length PKCδ as determined using the protein homology analogy recognition engine V 2.0 (PHYRE2). Solvent exposed surface is gray; $Thr^{505}$ is magenta; $His^{197}$ is blue; and $Cys^{200}$, $Cys^{393}$ and $Cys^{509}$ are yellow. Left image: full-length protein with potential zinc-binding pocket in color; middle image: close up of potential zinc-binding pocket; right image: potential zinc-binding residues rendered as sticks. (C) Molecular model of full-length PKCδ as determined using the protein homology analogy recognition engine V 2.0 (PHYRE2) bound to zinc (green). Solvent exposed surface is gray; zinc ion is green; $Thr^{505}$ is highlighted in magenta; $His^{197}$ is blue; and $Cys^{200}$, $Cys^{393}$ and $Cys^{509}$ are yellow. Left image: full-length protein with occluded zinc-binding pocket in color; middle image: close up of zinc-binding pocket; right image: zinc-binding residues rendered as sticks. Distances from electron donors to the zinc ion are shown in angstroms.

had high confidence for zinc binding.

To further understand the influence of zinc on the phosphorylation state of PKCδ at $Thr^{505}$ we generated a three-dimensional model of PKCδ. To the best of our knowledge, no crystal structure of PKCδ currently exists; we therefore employed the protein fold recognition server PHYRE2 to develop a three-dimensional molecular model of PKCδ. The PHYRE2 program uses advanced remote homology detection methods to build 3D models of proteins with known primary sequences [51]. Our model was generated by uploading the sequence of full-length PKCδ (residues 1–676, UniProtKB - Q05655) to the PHYRE2 server. The resulting model was rendered in PyMOL and a $Zn^{2+}$ pseudoatom was added near the $Thr^{505}$ residue. Interestingly, this site contains proximal residues including $His^{197}$, $Cys^{200}$, $Cys^{393}$ and $Cys^{509}$, with zinc binding predictions scores of 0.91 for $His^{197}$, 0.79 for $Cys^{200}$, 0.46 for $Cys^{509}$ and 0.23 for $Cys^{393}$; with $His^{197}$ and $Cys^{200}$ receiving high-confidence zinc-binding scores (Fig. 4A). These amino acids represent a potentially novel His-Cys3 zinc-binding domain [52]. Following addition of the pseudoatom, the resulting apo- and holo-protein models were subjected to energy minimization using the Swiss PDB Viewer server [53]. The minimized protein structures were then rendered and visualized using PyMOL molecular modeling software (Fig. 4B and C). Distance measurements on the zinc-bound model revealed that the zinc atom sits 4.6 Å from $His^{197}$, 3.7 Å from $Cys^{200}$, 4.3 Å from $Cys^{393}$ and 5.1 Å from $Cys^{509}$ (Fig. 4C, panel on the right). It should be noted that these are

approximate distance values generated using a computer model system and may not reflect actual interatomic distances found in the natural protein. Nevertheless, these results provide intriguing evidence of a potential PKCδ zinc-binding domain that has not been reported previously. Analysis of the solvent exposed surface of the apo-protein (no zinc) revealed that $Thr^{505}$ was exposed to the solvent, which exposes this site to the cytosol, and give access to other kinases to phosphorylate that site (Fig. 4B). However, the holo-protein (zinc-bound) displayed a markedly different structure near the $Thr^{505}$ residue with $His^{197}$ pointed toward the zinc atom, effectively occluding $Thr^{505}$ from the solvent exposed surface (Fig. 4C). These results strongly suggest that when PKCδ is bound to zinc at the $His^{197}$, $Cys^{200}$, $Cys^{393}$ and $Cys^{509}$ site, the ability of other kinases to phosphorylate $Thr^{505}$ may be significantly diminished. This model shows a novel mechanism by which zinc can directly influence the phosphorylation state of a protein.

## 4. Discussion

Despite extensive research, many fundamental aspects of PKCδ activation remain to be elucidated. This is likely due to complex regulatory mechanisms, including phosphorylation state and subcellular localization, which control activation of this enzyme. In this study, we applied a method to treat cultured HeLa cells with exogenous zinc and showed that the phosphorylation state and subcellular localization of PKCδ is influenced by the presence of intracellular free zinc. More specifically, we demonstrated that intracellular free zinc inhibits phosphorylation of PKCδ at $Thr^{505}$ in a concentration-dependent manner and that the presence of zinc facilitates targeting of PKCδ from cytosol to the Golgi complex. Furthermore, we employed molecular modeling to elucidate how zinc binds PKCδ and inhibits phosphorylation at $Thr^{505}$. These studies indicated that zinc may bind to a previously undocumented His-Cys3 binding site that is proximal to $Thr^{505}$. Upon zinc binding, it was observed that the imidazole ring of $His^{197}$ may orient itself in such a way that precludes phosphorylation at $Thr^{505}$. Thus, we propose a novel mechanism by which PKCδ is able to "sense" the changing concentration of intracellular zinc. Collectively, these results indicate that zinc binding may have a two primary effects on kinase activity: 1) inhibiting phosphorylation of PKCδ at $Thr^{505}$ and 2) facilitating PKCδ translocation to the Golgi complex. These new findings may help to enhance our understanding of diseases that are marked by changes in normal zinc homeostasis, including how zinc acts to modulate PKCδ phosphorylation and how cells respond to pathophysiological levels of intracellular zinc.

The detrimental effects and pathophysiological responses of intracellular zinc increase are well-documented [37–40, 54, 55]. However, many disease states induce cellular signaling events involving many independent factors that are often difficult to interpret in the context of a complex physiological response. Nevertheless, by increasing only intracellular zinc levels, we can begin to tease apart the role that zinc plays in these responses without the interference of other signals. We hypothesized that applying zinc in the presence of a zinc ionophore will mimic endogenous conditions of pathological zinc increases and help elucidate how zinc increase can influence PKCδ. To ensure that this method reliably increases intracellular zinc, we used a well-established intracellular free/labile zinc indicator FluoZin-3, AM. The benefits of labeling live cells in this manner is that we can observe changes in intracellular zinc in real time. HeLa cells showed a significant increase in intracellular zinc levels within the first minute of applying extracellular zinc and this increase was sustained through the duration of experiment (30 min). Thus, we propose that co-treatment with pyrithione and zinc is a suitable method to study intracellular zinc increases in cultured HeLa cells. However, this method has some limitations. For example, it is difficult to quantify the exact concentration of intracellular zinc and to determine whether this concentration remained within normal physiological range. Nonetheless, the data presented in this study is useful for adding to our understanding of how zinc affects cellular signaling networks that include PKCδ and will help elucidate the complex role zinc may play in regulating PKCδ activity and the cells stress response.

It is likely that the subcellular localization of PKCδ influences its function because the kinase has access to different protein substrates within different areas of the cell. In this study, we evaluated how levels of intracellular zinc affect the subcellular location of PKCδ. To accomplish this, we compared cells that had normal intracellular zinc levels to cells that were treated with exogenous zinc. We used a similar method to induce intracellular zinc increase as in the FluoZin-3, AM fluorescence experiments by application of exogenous zinc in combination with a zinc ionophore. For these studies, we employed a centrifugal fractionation method to separate cytosolic proteins from organelles and plasma membrane proteins. This fractionation method used consecutive centrifugations of whole cell lysates to separate proteins by subcellular localization. These experiments revealed that exposure to zinc causes PKCδ to translocate from the cytosol to organelle and membrane compartments. On the other hand, cells that were not exposed to zinc had the majority of PKCδ localized to the cytosol, with very little found in the organelles or membranes. While this method clearly showed that intracellular zinc influences trafficking of PKCδ, it was unclear what specific organelle PKCδ translocates to following zinc exposure. To determine precisely where PKCδ translocates under these conditions, we evaluated similarly treated cells by immunofluorescence. Treated cells were fixed and labeled with antibodies specific for PKCδ and then counter-stained with fluorescently-labeled antibodies specific for those targeting PKCδ. These experiments showed that PKCδ localized to the cytosol in the absence of zinc and to a distinct perinuclear compartment in cells treated with zinc. Subsequent immunofluorescence experiments using antibodies against the Golgi-specific protein β-COP revealed that PKCδ localizes to the Golgi following treatment with zinc. These data suggest that intracellular zinc increase influences PKCδ targeting to the Golgi complex. Previous studies have shown that PKCδ translocates to the Golgi complex in response to apoptotic signals [15], indicating that increases in intracellular zinc concentrations may stimulate apoptosis in HeLa cells. However further studies are need to address whether such zinc exposure induces apoptosis in HeLa cells.

In addition to its subcellular localization, the phosphorylation state of PKCδ is also known to play a critical role in the activity and function of this kinase. In this study, we investigated the effect zinc had on the phosphorylation state of $Thr^{505}$. This particular site is notable because it has been suggested to influence substrate specificity [19]. Furthermore, this site distinguishes PKCδ from other members of the 'novel kinase' family in that PKCδ is the only member that does not require this site to be phosphorylated for activation [56]. To evaluate the influence that intracellular zinc increase has on the phosphorylation state of $Thr^{505}$, we treated HeLa cells as described above and quantified levels of phosphorylated PKCδ ($pThr^{505}$) by western blot. Our results indicate that when intracellular zinc increases, the phosphorylation of PKCδ is inhibited. This result was concentration-dependent, with higher zinc treatment concentrations translating into greater inhibition of phosphorylation. Other groups have proposed that phosphorylation at $Thr^{505}$ can influence substrate specificity [19]. Therefore, we suggest that zinc plays a role in regulating the activity and specificity of PKCδ, and may ultimately change cell fate.

We envision several independent, or perhaps concerted, scenarios where the phosphorylation status of $Thr^{505}$ could be influenced by intracellular concentrations of free zinc. For example, increases in intracellular zinc may inhibit kinases that phosphorylate $Thr^{505}$ or stimulate the activation of phosphatases that dephosphorylate $Thr^{505}$. Another possibility is that intracellular free zinc may directly hinder the phosphorylation of $Thr^{505}$ by binding to a zinc-binding site adjacent to the $Thr^{505}$ residue. To further explore the latter possibility, we employed molecular modeling software such as PHYRE2 and PyMOL to generate a folded structure of full-length PKCδ and evaluated how

possible zinc binding could influence phosphorylation at $Thr^{505}$. Our modeling efforts were initiated by assigning zinc binding prediction scores to each residue of the full-length PKCδ protein using the zinc binding prediction engine ZincExplorer. A total of 16 amino acids were determined to have zinc binding potential, interpreted as having zinc binding prediction scores greater than or near 0.49. We then generated a folded model of PKCδ by uploading its primary sequence (residues 1–676, UniProtKB - Q05655) to the PHYRE2 server. Interestingly, this folded model was observed to contain a potential His-Cys3 zinc binding site near $Thr^{505}$, consisting of $His^{197}$, $Cys^{200}$, $Cys^{393}$ and $Cys^{509}$. Three of the residues $His^{197}$, $Cys^{200}$ and $Cys^{509}$ each had zinc binding prediction scores greater than 0.49 indicating a high probability for binding zinc. When a zinc pseudoatom was placed near this binding pocket and the structure was energy minimized, it was observed that the donor residues were repositioned at distances between 4.6 and 5.4 Å from the zinc ion. Notably, when the solvent exposed surface was analyzed, it appeared that the presence of the zinc ion causes the $His^{197}$ residue to essentially close the zinc binding pocket and occlude $Thr^{505}$ from the solvent. The zinc-mediated reorientation of $His^{197}$ provides a rational mechanism for how zinc binding inhibits phosphorylation of $Thr^{505}$ in PKCδ. We therefore hypothesize that when intracellular zinc concentration increases, PKCδ will bind zinc at $His^{197}$, $Cys^{200}$, $Cys^{393}$ and $Cys^{509}$, and this interaction will directly prevent further phosphorylation of $Thr^{505}$. This modification may also influence the intracellular targeting and function of PKCδ. Indeed, it has been shown previously that T505A mutations cause PKCδ to translocate to cellular compartments similar to the Golgi complex [57].

In summary, we have studied the effect intracellular zinc increase has on the phosphorylation state and subcellular localization of PKCδ. Our results indicate that short exposure (less than 30 min) of HeLa cells to exogenous zinc inhibits the phosphorylation of PKCδ at $Thr^{505}$. We also showed that zinc influences the subcellular targeting of PKCδ, where increases in intracellular zinc facilitates translocation of PKCδ to the Golgi complex. It should be noted that these data alone are not wholly sufficient to elucidate whether intracellular zinc directly causes dephosphorylation and translocation of PKCδ to the Golgi complex. However, we propose here a novel mechanism by which PKCδ can bind zinc ions that would preclude phosphorylation of $Thr^{505}$. Molecular modeling simulations have provided a rational for how PKCδ can use a novel His-Cys3 zinc-binding pocket to 'sense' intracellular concentrations of free zinc and respond to changes in zinc homeostasis. These findings indicate that zinc, and possibly other transition metals, may play a distinct role in regulating the activity of 'novel kinases' and should provide a basis for future studies investigating cellular processes that rely on metal ion-protein interactions.

## 5. Conclusions

We have identified a novel effector of PKCδ phosphorylation to be free zinc. This work demonstrated the intracellular zinc increase causes concentration dependent inhibition of phosphorylation of PKCδ at activation loop site $Thr^{505}$ and changes the subcellular localization of PKCδ from cytosolic to Golgi complex.

## Author contributions

KGS conceived the study, performed experiments and researched data, wrote the manuscript, generated the figures and references. JMH researched and performed the computer modeling, generated the computer modeling figures, contributed to discussions, reviewed and edited the manuscript and added references. YVL coordinated the study, secured the funding, contributed to discussions and reviewed the manuscript. All authors approved the final version of the manuscript.

## Conflict of interest

The authors declare that they have no conflict of interests.

## Acknowledgment

The authors would like to thank Zihui Wang for assisting with zinc fluorescence experiments and helpful discussions about metal ion-amino acid interactions. The authors would also like to acknowledge Yuli Hu for help with phospho-immunoblots and helpful discussions. Dr. Ramiro Malgor assisted with immunofluorescence microscopy and provided the equipment as well as insightful discussions about co-localization of PKCδ and Golgi complex. Finally, the authors would like to thank Dr. Mark Berryman, for assisting with compartmentalization experiments, generously providing instrumentation support and gifting antibodies for immunofluorescence experiments of Golgi apparatus. This research was supported in part by a NIH grant NS081629 to YVL.

## References

[1] W.C. Wetsel, et al., Tissue and cellular distribution of the extended family of protein kinase C isoenzymes, J. Cell Biol. 117 (1) (1992) 121–133.
[2] H. Leibersperger, et al., Immunological demonstration of a calcium-unresponsive protein kinase C of the delta-type in different species and murine tissues. Predominance in epidermis, J. Biol. Chem. 266 (22) (1991) 14778–14784.
[3] A.W. Ashton, et al., Protein kinase Cδ inhibition of S-phase transition in capillary endothelial cells involves the cyclin-dependent kinase inhibitor p27Kip1, J. Biol. Chem. 274 (30) (1999) 20805–20811.
[4] K. Kitamura, et al., The second phase activation of protein kinase Cδ at late G1 is required for DNA synthesis in serum-induced cell cycle progression, Genes Cells 8 (4) (2003) 311–324.
[5] K.C. Corbit, D.A. Foster, M.R. Rosner, Protein kinase Cδ mediates neurogenic but not mitogenic activation of mitogen-activated protein kinase in neuronal cells, Mol. Cell. Biol. 19 (6) (1999) 4209–4218.
[6] C. Brodie, P. Blumberg, Regulation of cell apoptosis by protein kinase Cδ, Apoptosis 8 (1) (2003) 19–27.
[7] T. Kajimoto, et al., Ceramide-induced apoptosis by translocation, phosphorylation, and activation of protein kinase Cδ in the Golgi complex, J. Biol. Chem. 279 (13) (2004) 12668–12676.
[8] D.N. Jackson, D.A. FOSTER, The enigmatic protein kinase Cδ: complex roles in cell proliferation and survival, FASEB J. 18 (6) (2004) 627–636.
[9] A.C. Newton, Protein kinase C: seeing two domains, Curr. Biol. 5 (9) (1995) 973–976.
[10] M. Freeley, D. Kelleher, A. Long, Regulation of protein kinase C function by phosphorylation on conserved and non-conserved sites, Cell. Signal. 23 (5) (2011) 753–762.
[11] S. Jaken, Protein kinase C isozymes and substrates, Curr. Opin. Cell Biol. 8 (2) (1996) 168–173.
[12] A. Basu, D. Pal, Two faces of protein kinase Cδ: the contrasting roles of PKCδ in cell survival and cell death, Sci. World J. 10 (2010) 2272–2284.
[13] R. Gomel, et al., The localization of protein kinase Cδ in different subcellular sites affects its proapoptotic and antiapoptotic functions and the activation of distinct downstream signaling pathways, Mol. Cancer Res. 5 (6) (2007) 627–639.
[14] M.E. Reyland, Protein kinase C isoforms: multi-functional regulators of cell life and death, Frontiers in bioscience (Landmark edition) (14) (2009) 2386.
[15] T. Kajimoto, et al., Subtype-specific translocation of the δ subtype of protein kinase C and its activation by tyrosine phosphorylation induced by ceramide in HeLa cells, Mol. Cell. Biol. 21 (5) (2001) 1769–1783.
[16] P.K. Majumder, et al., Targeting of protein kinase C delta to mitochondria in the oxidative stress response, Cell Growth & Differentiation: The Molecular Biology Journal of the American Association for Cancer Research 12 (9) (2001) 465–470.
[17] S.F. Steinberg, Distinctive activation mechanisms and functions for protein kinase Cδ, Biochem. J. 384 (3) (2004) 449–459.
[18] A. Welman, et al., Protein kinase C delta is phosphorylated on five novel Ser/Thr sites following inducible overexpression in human colorectal cancer cells, Protein Sci. 16 (12) (2007) 2711–2715.
[19] Y. Liu, et al., Independence of protein kinase C-δ activity from activation loop phosphorylation structural basis and altered functions in cells, J. Biol. Chem. 281 (17) (2006) 12102–12111.
[20] M.P. Sumandea, et al., Tyrosine phosphorylation modifies protein kinase Cδ-dependent phosphorylation of cardiac troponin I, J. Biol. Chem. 283 (33) (2008) 22680–22689.
[21] M. Vašák, D.W. Hasler, Metallothioneins: new functional and structural insights, Curr. Opin. Chem. Biol. 4 (2) (2000) 177–183.
[22] L. Rink, Zinc and the immune system, Proc. Nutr. Soc. 59 (4) (2000) 541–552.
[23] D. Beyersmann, Homeostasis and cellular functions of zinc, Mater. Werkst. 33 (12) (2002) 764–769.
[24] A. Krezel, W. Maret, The biological inorganic chemistry of zinc ions, Arch. Biochem. Biophys. 611 (2016) 3–19.
[25] M. Stefanidou, et al., Zinc: a multipurpose trace element, Arch. Toxicol. 80 (1)

(2006) 1.
[26] C.T. Chasapis, et al., Zinc and human health: an update, Arch. Toxicol. 86 (4) (2012) 521–534.
[27] Q. Lu, et al., Intracellular zinc distribution in mitochondria, ER and the Golgi apparatus, International Journal of Physiology, Pathophysiology and Pharmacology 8 (1) (2016) 35.
[28] W. Maret, Analyzing free zinc (II) ion concentrations in cell biology with fluorescent chelating molecules, Metallomics 7 (2) (2015) 202–211.
[29] L.A. Lichten, R.J. Cousins, Mammalian zinc transporters: nutritional and physiologic regulation, Annu. Rev. Nutr. 29 (2009) 153–176.
[30] E. John, et al., Zinc in innate and adaptive tumor immunity, J. Transl. Med. 8 (1) (2010) 118.
[31] C.-Y. Wang, et al., Zinc overload enhances APP cleavage and Aβ deposition in the Alzheimer mouse brain, PLoS One 5 (12) (2010) e15349.
[32] P.S. Donnelly, et al., Selective intracellular release of copper and zinc ions from bis (thiosemicarbazonato) complexes reduces levels of Alzheimer disease amyloid-β peptide, J. Biol. Chem. 283 (8) (2008) 4568–4577.
[33] A. Takeda, Zinc signaling in the hippocampus and its relation to pathogenesis of depression, J. Trace Elem. Med. Biol. 26 (2) (2012) 80–84.
[34] J. Lai, et al., The efficacy of zinc supplementation in depression: systematic review of randomised controlled trials, J. Affect. Disord. 136 (1) (2012) e31–e39.
[35] F. Chimienti, et al., In vivo expression and functional characterization of the zinc transporter ZnT8 in glucose-induced insulin secretion, J. Cell Sci. 119 (20) (2006) 4199–4206.
[36] G.A. Rutter, Think zinc: new roles for zinc in the control of insulin secretion, Islets 2 (1) (2010) 49–50.
[37] C.J. Frederickson, W. Maret, M.P. Cuajungco, Zinc and excitotoxic brain injury: a new model, Neuroscientist 10 (1) (2004) 18–25.
[38] Y.V. Medvedeva, et al., Intracellular $Zn^{2+}$ accumulation contributes to synaptic failure, mitochondrial depolarization, and cell death in an acute slice oxygen–glucose deprivation model of ischemia, J. Neurosci. 29 (4) (2009) 1105–1114.
[39] C.J. Stork, Y.V. Li, Rising zinc: a significant cause of ischemic neuronal death in the CA1 region of rat hippocampus, J. Cereb. Blood Flow Metab. 29 (8) (2009) 1399–1408.
[40] K. Slepchenko, Y.V. Li, Cross-talks between intracellular zinc increases and reactive oxygen species in hypoxia, FASEB J. 31 (1 Supplement) (2017) 779.6.
[41] A. Boom, et al., Bimodal modulation of tau protein phosphorylation and conformation by extracellular $Zn^{2+}$ in human-tau transfected cells, Biochimica et Biophysica Acta (BBA)-Molecular Cell Research 1793 (6) (2009) 1058–1067.
[42] J.M. Samet, et al., Mechanisms of $Zn^{2+}$-induced signal initiation through the epidermal growth factor receptor, Toxicol. Appl. Pharmacol. 191 (1) (2003) 86–93.
[43] S. Lee, et al., Molecular mechanism underlying Akt activation in zinc-induced cardioprotection, Am. J. Phys. Heart Circ. Phys. 297 (2) (2009) H569–H575.
[44] B. Ahluwalia, et al., Zinc inhibits protein phosphorylation in isolated sperm head membranes in *Spisula solidissima*, Andrologia 23 (2) (1991) 121–126.
[45] K.R. Gee, et al., Measuring zinc in living cells.: a new generation of sensitive and selective fluorescent probes, Cell Calcium 31 (5) (2002) 245–251.
[46] A.S. Gordon, et al., Ethanol alters the subcellular localization of δ-and ε protein kinase C in NG108–15 cells, Mol. Pharmacol. 52 (4) (1997) 554–559.
[47] M. Humphries, et al., Tyrosine phosphorylation regulates nuclear translocation of PKCδ, Oncogene 27 (21) (2008) 3045.
[48] A. Zrachia, et al., Infection of glioma cells with Sindbis virus induces selective activation and tyrosine phosphorylation of protein kinase Cδ implications for Sindbis virus-induced apoptosis, J. Biol. Chem. 277 (26) (2002) 23693–23701.
[49] J.G. Donaldson, et al., Binding of ARF and beta-COP to Golgi membranes: possible regulation by a trimeric G protein, Science 254 (5035) (1991) 1197–1199.
[50] Z. Chen, et al., ZincExplorer: an accurate hybrid method to improve the prediction of zinc-binding sites from protein sequences, Mol. BioSyst. 9 (9) (2013) 2213–2222.
[51] L.A. Kelley, et al., The Phyre2 web portal for protein modeling, prediction and analysis, Nat. Protoc. 10 (6) (2015) 845–858.
[52] M.T. Worthington, et al., Metal binding properties and secondary structure of the zinc-binding domain of Nup475, Proc. Natl. Acad. Sci. U. S. A. 93 (24) (1996) 13754–13759.
[53] N. Guex, M.C. Peitsch, SWISS-MODEL and the Swiss-Pdb viewer: an environment for comparative protein modeling, Electrophoresis 18 (15) (1997) 2714–2723.
[54] Y.V. Medvedeva, J.H. Weiss, Intramitochondrial $Zn^{2+}$ accumulation via the $Ca^{2+}$ uniporter contributes to acute ischemic neurodegeneration, Neurobiol. Dis. 68 (2014) 137–144.
[55] K.G. Slepchenko, Q. Lu, Y.V. Li, Zinc wave during the treatment of hypoxia is required for initial reactive oxygen species activation in mitochondria, International Journal of Physiology, Pathophysiology and Pharmacology 8 (1) (2016) 44.
[56] V.O. Rybin, et al., Stimulus-specific differences in protein kinase Cδ localization and activation mechanisms in cardiomyocytes, J. Biol. Chem. 279 (18) (2004) 19350–19361.
[57] T. Seki, et al., Phosphorylation of PKC activation loop plays an important role in receptor-mediated translocation of PKC, Genes Cells 10 (3) (2005) 225–239.